Substrate Integrated Waveguide - Dielectric Resonator Antenna for Future Wireless Communication

Emmanuel K. Chemweno, Pradeep Kumar, and Thomas J. O. Afullo, Senior *Member, IEEE*

***Abstract*— A substrate integrated waveguide (SIW) fed rectangular-shaped dielectric resonator antenna (DRA) is proposed for application in the D - Band frequency regime. The Dielectric Resonator (DR) is designed to operate in higher order modes. A rectangular-shaped narrow slot is used to excite the DR element, leading to multiple resonances. The resulting structure is a multi-resonant antenna operating at six frequencies at 123.64 GHz, 125.76 GHz, 127.4 GHz, 129.9 GHz, 134.9 GHz and 137.7 GHz frequencies. These are identified as $TE_{10\delta1}$, $TE_{7\delta5}$, $TE_{\delta31}$, $TE_{\delta25}$, $TE_{\delta31}$ and $TE_{\delta35}$ modes of operation of the resonator, respectively. These resonances are merged to achieve a -10 dB impedance bandwidth ranging between 122.58 GHz and 139.51 GHz, equivalent to 13.4% at a center frequency of 125.76 GHz. Moreover, the antenna possesses a stable radiation pattern in the broadband direction, across the entire frequency band of operation. Simulation results show that the antenna has a peak gain of 12.3 dBi, maximum directivity of 13.14 dBi and maximum efficiency of 84% at a frequency of 126 GHz. Simulated results show that the proposed design has potential and suitability for utilization in future wireless communications.**

***Index Terms*— Dielectric Resonator Antenna (DRA), millimeter (mm) waves, Substrate Integrated Waveguide (SIW), Terahertz (THz)**

I. Introduction

In the recent past, there has been increased global focus towards the creation of a sustainable society. Advances in science and technology have seen an increase in computing power, speed and storage capacity of electronic systems. These have in turn led to the innovation of services and technologies such as internet of things (IoT), artificial intelligence (AI), cloud computing, big data, machine-to-machine (M2M) communication, etc. In anticipation towards the creation of a "super-smart society", an initiative dubbed Society 5.0 was proposed in 2016 by the Japanese government [1]. This concept finds leverage in these enabling technologies, which have greatly integrated the physical space and cyberspace.

Wireless communication forms an integral part of this paradigm towards the creation of a human-centered society. The 5G wireless network connectivity laid the foundation for the initial deployment of these applications. The large amount of data traffic associated with the 5G networks is projected to increase at a very rapid pace. This explosive growth in the number of end-user devices and sensors that support IoT applications is anticipated to expose the inherent limitations in the 5G networks [2]. Consequently, this has dictated stringent requirements in the capabilities of future generation mobile networks such as high data rates, high reliability, ultra-low latency and wide bandwidths. This is expected to explore more spectrum in the high frequency bands.

The terahertz (THz) frequency spectrum is a high frequency band defined at 0.1-10 THz. This spectrum is projected to offer speeds up to terabits per second (Tbps), capable of meeting this capacity demand as well as provide low latency communications [3]. There has been increased research in the area of terahertz communications systems and technologies in the recent past. Antennas form an integral part of communication systems because they provide an interface to couple electromagnetic energy to free space. Therefore, a good antenna design is critical for overall system performance. This article focuses on the design of a high performance antenna to meet the requirements of future wireless communication systems.

At high frequencies, the conventional microstrip patch antennas (MPAs) suffer from low gain, poor radiation efficiency and narrow bandwidth [4], [5]. Dielectric resonator antennas (DRAs) offer a suitable structure with attractive attributes such as small size, low profile and high radiation efficiency [6], [7]. These make them suitable as antenna elements for millimeter waves and terahertz systems. Besides, the DRA exhibits different radiation characteristics depending on the different modes of operation of the resonator [6]. Owing to their larger effective aperture, DRAs exhibit a wider impedance bandwidth as compared to conventional MPAs [8]. To enhance the DRA bandwidth, a number of innovative techniques have been reported. These include the use of low

E. K. Chemweno is with the Discipline of Electrical, Electronic and Computer Engineering, Howard College Campus, University of KwaZulu-Natal, Durban, South Africa. (E-mail ce_kiprop@yahoo.co.uk)

P. Kumar is with the Discipline of Electrical, Electronic and Computer Engineering, Howard College Campus, University of KwaZulu-Natal, Durban, South Africa. (E-mail pkumar_123@yahoo.com)

T. J. O. Afullo is with the Discipline of Electrical, Electronic and Computer Engineering, Howard College Campus, University of KwaZulu-Natal, Durban, South Africa. (E-mail afullot@ukzn.ac.za)

dielectric constant materials, stacking of different DR elements, modification of the resonator geometrical shape, modification of the feeding structures, operating the DRA in a higher order mode among others.

Wide impedance bandwidths can be achieved by operating the DRs in higher order modes. The mode distribution of a rectangular DRA (RDRA) is affected by its aspect ratio (height/length and width/length). The aspect ratios for a rectangular DR can be independently chosen to provide better bandwidth control [9], [10]. The use of structural discontinuities by drilling of holes and the use of wells and moats in the DR have been analyzed in [4], [8]. These have the effect of reducing the Q-factor of the DR to achieve an increase in the bandwidth. The use of modified DR geometries has been applied in [5], where the authors have used a fractal structure in the DR element to achieve a bandwidth of 19.5%. The effect of this fractal geometry is to introduce air gaps in the element. This causes a reduction in the effective permittivity, thus broadening the bandwidth. Modification of the feeding structure to enhance the bandwidth has also been reported. In [11], the shape of the feeding slot has been modified to form a cross shape to enhance the bandwidth from 5% to 8.8%. Other feeding structures reported in literature include the on-chip half mode SIW (HMSIW) [12] and the SIW cavity-backed antennas [13]. Combination of two or more techniques has also been proposed. Besides using a cross-slot feed structure, Yang *et al* [13] have also designed a multilayered substrate antenna, with a modified cylindrical DRA element to achieve an impedance bandwidth of 34.6%. SIW-fed DRAs have been applied to design antennas in [14] and [15] where the designers have achieved single and dual-band operations respectively. Some of the bandwidth enhancement techniques may lead to complexity both in the fabrication process and in the overall antenna structure. Consequently, the desirable attributes of amenability to planar structures and miniaturization may not be achieved.

To couple the DR to the electromagnetic energy source, conventional feeding methods such as coaxial probes, microstrip lines, slot lines or coplanar feeds have been employed. However, these methods suffer high radiation losses [11] and thus are not suitable for application at the mm-wave and THz frequencies. Substrate integrated waveguides (SIWs) offer a convenient way of integration of the antenna into planar structures. It offers the advantage that the fields are confined within the guiding SIW structure, thus minimizing radiation losses in the feeding structure.

In this work, we present a SIW-fed DRA operating in the D – band frequency spectrum. The use of higher order cavity resonance has been reported in [16] to enhance the gain of SIW cavity-backed antennas. We extend the use of a higher order cavity to design the SIW feeding structure. The DR element is designed to operate in higher order modes. The antenna is thus designed to achieve a higher bandwidth by merging the multimode resonances of the resonator.

This paper is organized as follows. Section II discusses the details of the antenna design. Section III presents the simulation results and the description of the performance of the antenna. Finally, Section IV gives the conclusion of this work.

II. ANTENNA DESIGN

The proposed design of the antenna involves the designs of both the feed structure and the radiating element. The details of the designs are presented in this section:

A. SIW Design

Fig. 1 shows the geometry of a DR element fed from a SIW through an aperture slot. The SIW feed is designed from RT Duroid 5880 substrate material of dielectric constant $\epsilon_r = 2.2$, a loss tangent of $\delta = 0.0009$ and a substrate height of $h = 0.254$. The thin substrate is chosen to ensure low loss and wider bandwidth of operation [17]. The SIW guides the electromagnetic waves by confining it between the two rows of metalized via posts. Due to lack of longitudinal surface currents as a result of the gaps formed by the vias, the structure supports TE_{m0} modes (m integer).

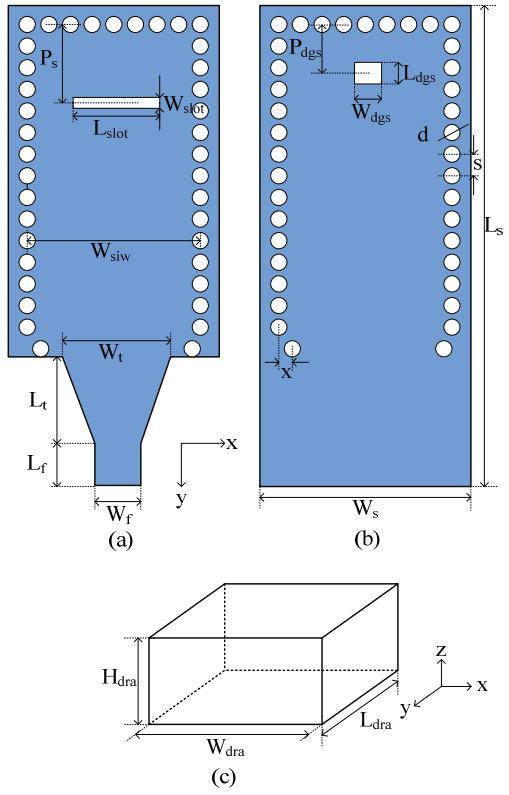

Fig 1. The geometry of the proposed SIW-fed DRA showing (a) the top view (b) the ground plane and (c) the DRA element

The via to via width of the SIW is initially determined by mapping the dimensions of a D – band rectangular WR-6 metallic waveguide to achieve the same cut-off frequency f_c at the lowest TE_{10} mode. The cut-off frequency for propagating modes in a rectangular waveguide of sides a and b $(a > b)$ filled with a material of permittivity ϵ_r is given by [18]:

$$f_{c,mn} = \frac{c}{2\sqrt{\epsilon_r}}\sqrt{\left(\frac{m}{a}\right)^2 + \left(\frac{n}{b}\right)^2} \quad (1)$$

Where:
m, n are mode indices and c the speed of light.
The effective width of a SIW (W_{siw}) of via diameter d and pitch s is using the empirical equations given in [19] as:

$$a = W_{siw} - 1.08\frac{d^2}{s} + 0.1\frac{d^2}{W_{siw}} \quad (2)$$

This effective width ensures the waveguide operates in the fundamental TE_{10} mode in this frequency range. To enable the cavity operate in a higher order mode, this width of the SIW is scaled by an integer factor. Further, to ensure confinement of the TE fields and minimize the radiation along the walls, as well as minimize bandgap effects, d and s are selected according to the following rules: $s \leq 2d$ and $d \leq \lambda_g/5$, where λ_g is the guided wavelength [20]. The value of s and d is chosen large enough. One end of the SIW is terminated in a short circuit by use of via while the opposite end is connected to the feed-line.

A linearly tapered microstrip transition of length L_T and width W_T is used to match the resonator structure to the 50Ω feeding line. The dimensions of this taper are optimized over the operating frequency to achieve broadband matching.

A rectangular-shaped slot of sides L_{slot} and W_{slot} is etched from the top conductor of the SIW cavity. This aperture forms a central feeding slot for the DR element. The position from the short-circuited end of the resonator to the center of the slot is initially determined from $P_s = n\lambda_g/4$, (n odd). This point corresponds to maximum standing wave field intensity and thus the slot achieves good energy coupling.

A Defected ground structure (DGS) of length L_{dgs} and width W_{dgs} is etched out from the ground plane of the SIW cavity at a position P_{dgs}. DGSs have the effect of altering the shield current distribution. Due to these defect(s), the transmission line characteristics (capacitance and inductance) of the structure are altered [21]. DGS have been used in conventional MPAs to enhance gain, suppress cross-polarization to improve polarization purity and broaden the bandwidth, through improved impedance matching. In the proposed design, we apply the use of DGS technique on a SIW cavity to increase the bandwidth of the antenna.

To improve further the impedance matching in this frequency band, two vias are offset with respect to the row of vias by a distance x.

B. DRA Design

The DR element is chosen from 99.5% Alumina dielectric material with a dielectric constant of $\epsilon_{rd} = 9.8$. A rectangular-shaped DR is preferred because of the higher degree of choice of the aspect ratio desirable for bandwidth control and to achieve desirable radiation characteristics. The physical dimensions of this element L_{dra}, W_{dra} and H_{dra} are selected to ensure higher mode operation of the DR. The resonant frequency of the DR element is determined by solving the transcendental equation of the dielectric waveguide model (DWM) given by [22]:

$$k_x \tan\left(\frac{k_x L_{dra}}{2}\right) = \sqrt{(\epsilon_{rd} - 1)k_{mn}^2 - k_x^2} \quad (3)$$

Where:
$k_x^2 + k_y^2 + k_z^2 = \epsilon_{rd} k_{mn}^2$, $f_{mn} = \frac{c}{2\pi\sqrt{\epsilon_{rd}}}\sqrt{k_x^2 + k_y^2 + k_z^2}$,
$k_y = \frac{m\pi}{W_{dra}}$, $k_z = \frac{n\pi}{H_{dra}}$

This element is placed atop the resonator structure to form the desired SIW-fed DRA. The elements of the antenna are simulated and optimized to achieve better performance.

III. SIMULATION RESULTS AND PERFORMANCE ANALYSIS

To simulate the proposed SIW-DRA, the structure was modeled in CST Microwave Studio. The different antenna parameters were selected according to section II above. These parameters were optimized for better antenna performance. Table I presents the optimized dimensions of the proposed antenna. The size of the SIW-DRA is 10.18×5.08 mm^2.

TABLE I
OPTIMIZED ANTENNA PARAMETERS

Parameter	Value	Description
d	Via diameter	0.29
h	Substrate height	0.254
H_{dra}	Resonator height	1.29
L_{dgs}	DGS length	0.4
L_{dra}	Resonator length	1.39
L_f	Feed length	0.3
L_s	Substrate length	10.18
L_{slot}	Slot length	1.8
L_t	Taper length	1.045
P_s	Slot position	2.48
P_{dgs}	DGS position	0.94
s	Via pitch	0.56
W_{dgs}	DGS width	0.42
W_{dra}	Resonator width	3.89
W_f	Feed width	0.67
W_s	Substrate width	5.08
W_{siw}	Effective SIW with	4.5
W_{slot}	Slot width	0.35
W_t	Taper width	0.85
x	Via offset position	0.1

All dimensions in millimeters

The slot is centrally placed with respect to the DR element to couple maximum energy from the cavity to excite higher order resonance in the DR element. Fig. 2 shows the simulated S_{11} performance of the SIW-DRA. The proposed design exhibits a multi-mode behavior operating in six distinct but closely lying resonant frequencies at 123.64 GHz, 125.76 GHz, 127.4 GHz, 129.9 GHz, 134.9 GHz and 137.7 GHz. An isolated DR element was simulated using the eigenmode solver of the CST to determine the modes that are excited in the DR. The modes of a rectangular resonator can be determined by observing the number of half-wave variations

of the E and H fields along the three orthogonal directions. To determine the modes excited in the DR, we briefly illustrate the analysis of the modes. For a rectangular-shaped DR shown in Fig. 1, only TE modes can be excited [23]. The modes supported are designated $TE^{x}_{m,n,p}$, $TE^{y}_{m,n,p}$ or $TE^{z}_{m,n,p}$ where the superscript indicates the direction of the orientation of the magnetic dipole and m, n, p are the mode indices, representing the number of half-wave field variations in the three directions. For geometries of the DR shorter than half wavelength, the mode indices may be written as $m + \delta$ or $n + \delta$ $(m, n = 0,1,2 \ldots)$ where $0 < \delta \leq 1$. When the DR element is placed on top of a ground plane, the even modes in the z – direction are extinguished [22]. In addition, the numerical value of δ is seldom needed, therefore, these modes may simply be denoted as $TE_{\delta,n,p}$ and $TE_{m,\delta,p}$ $(p = odd)$ for $x-$ and $y-$ directed short dipoles.

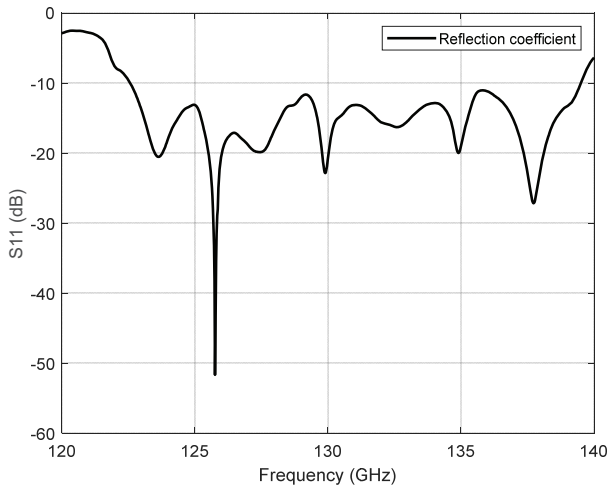

Fig 2. Simulated reflection coefficient of the SIW - DRA

Eigenmode simulation of an isolated DR element is used to determine the resonant modes of the DR. These modes are matched to the resonating frequencies to determine the excited modes. Fig. 3 shows the simulated H-fields showing the different modes excited in the DR element. The half-wave variations of the H fields in the $x-$, $y-$ and $z-$ directions indicate the excited modes at different resonant frequencies. The H-fields show that at these frequencies, the excited modes of the resonator are identified as $TE_{10\delta1}$, $TE_{7\delta5}$, $TE_{\delta31}$, $TE_{\delta25}$, $TE_{\delta31}$ and $TE_{\delta35}$, respectively. However, there is some slight frequency shifts between the resonant frequencies of the proposed design and those of the resonant modes of the DR element simulated using the eigenmode solver. Whereas the DWM model assumes an infinite ground plane for an isolated DR element, the effects of finite ground plane and that of the slot loading may cause the slight frequency shifts [24]. Simulated results show that the proposed antenna achieves a -10 dB bandwidth ranging from 122.58 GHz to 139.51 GHz, representing 13.4% at the center frequency of 125.76 GHz. This wideband operation is attributed to the merging together of the higher order resonances as a result of the judicious selection of the DR aspect ratios and improved impedance matching between the feed line and the SIW-DRA. To achieve the improved impedance matching, two techniques have been employed, *viz* use of a DGS on the ground plane conductor and offsetting of the vias at the resonator – taper interface.

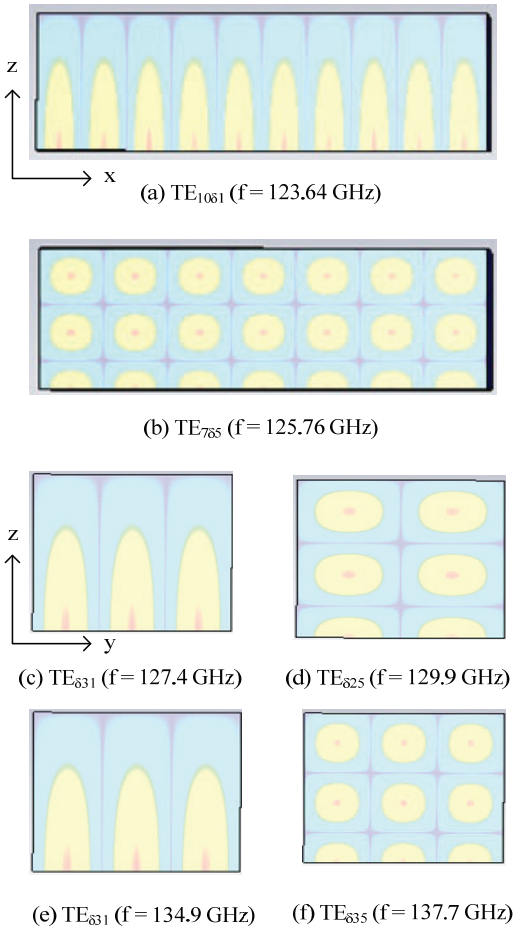

Fig 3. H-field distributions of the rectangular DRA element showing different modes excited at different resonant frequencies

TABLE II
FARFIELD CHARACTERISTICS OF THE ANTENNA AT DIFFERENT RESONANT FREQUENCIES

f_0	MLD	3dB BMW	Main Lobe Magnitude (dBi)				
	ABS	ABS	ABS	Co-pol		X-pol	
(GHz)	Deg	Deg	E	E	H	E	H
123.64	36°	30°	6.54	6.37	9.22	-5	-92
125.76	0°	25.8°	10.3	10.3	11.9	-2.69	-88.3
127.4	0°	46.5°	7.18	7.18	11.8	-2.58	-97.3
129.9	39°	121.4°	3.88	3.71	8.76	0.28	-90.6
134.9	61°	34.4°	4.48	3.68	6.28	-0.0736	-91.4
137.7	0°	31.5°	11	11	11.2	-5.19	-96.8

MLD – Main lobe direction, BMW – Beamwidth, ABS – Absolute, E – E-plane, H – H-plane, Co-pol – Co-polarization, Xpol-cross-polarization

The far-field radiation patterns of higher mode antenna can be predicted using short magnetic dipoles and has been shown to be broadband in nature [22]. The radiation patterns of the

individual resonant frequencies associated with each resonant mode is thus investigated. Each mode excited in the DR is defined by a unique field pattern. Therefore, each mode exhibits different radiation characteristics. Fig. 4 shows the simulated radiation characteristics at 123.64 GHz, 125.76 GHz, 127.4 GHz, 129.9 GHz, 134.9 GHz and 137.7 GHz resonant frequencies. It is observed that the radiation patterns are generally broadband with deviations in the direction of their main lobe maxima. For the E-plane ($\phi = 0^o$), these angles are given as 36^o, 0^o, 0^o, 39^o, 61^o and 0^o in the order of increasing resonant frequencies respectively. This difference in the direction of antenna main lobe magnitudes is attributed to the multi-mode nature of the antenna operation. Table II lists the far-field characteristics of the antenna at different resonant frequencies. It can be observed that the contribution of the "off-boresight" resonances to the overall antenna performance has been suppressed, as the resonance at these frequencies is not deep. This is explained from the reduced gains of 6.54 dBi at 123.64 GHz, 3.88 dBi at 129.9 GHz and 4.48 dBi at 134.9 GHz (as compared to 10.3 dBi at 125.76 dBi, 7.18 dBi at 127.4 GHz and 11.0 dBi at 137.7 GHz). Because of these similar broadband radiation characteristics, and the suppression of the otherwise degenerate modes, the resulting broadband response and the antenna performance is not significantly distorted but remains stable in the frequency band of operation.

The levels of co-polarized and cross-polarized components of the radiated fields are important in determining the polarization loss of the antenna. In particular, increase in cross-polarization fields leads to the degradation in radiation performance of the antenna. The use of higher order modes to achieve higher bandwidth has been attributed to increase in cross-polarized radiation in patch antennas [25] and dielectric resonators [26]. The radiation performance of the proposed design is further investigated through the observation of these fields. The levels of the co-polarized and cross-polarized fields for E- and H-planes are shown in Fig. 4 for the different resonant frequencies.

From the plot, the main lobe magnitudes for the cross-polarized fields in the E-plane are -5.0 dBi, -2.69 dBi, -2.58 dBi, 0.28 dBi, -0.0736 dBi and -5.19 dBi in the direction of increasing resonant frequencies respectively, while in the H-plane, these field magnitudes are -92 dBi, -88.3 dBi, -97.3 dBi,-90.6 dBi, -91.4 dBi and -96.8 dBi respectively. It can be observed that while the level of cross-polarized field component in the H- plane is greatly minimized with respect to the co-polarized fields, the contrary is true for the E plane. In the H plane, there is suppression of the degenerate modes with radiation patterns that would increase the level of cross-polarization, and distort the overall antenna radiation pattern. This is attributed to the similar radiation characteristics of the slot and that of the DR, which minimizes the cross-polarized fields [10]. The proposed design offers a poor cross-polarization performance in the E- plane, compared to that of the H-plane.

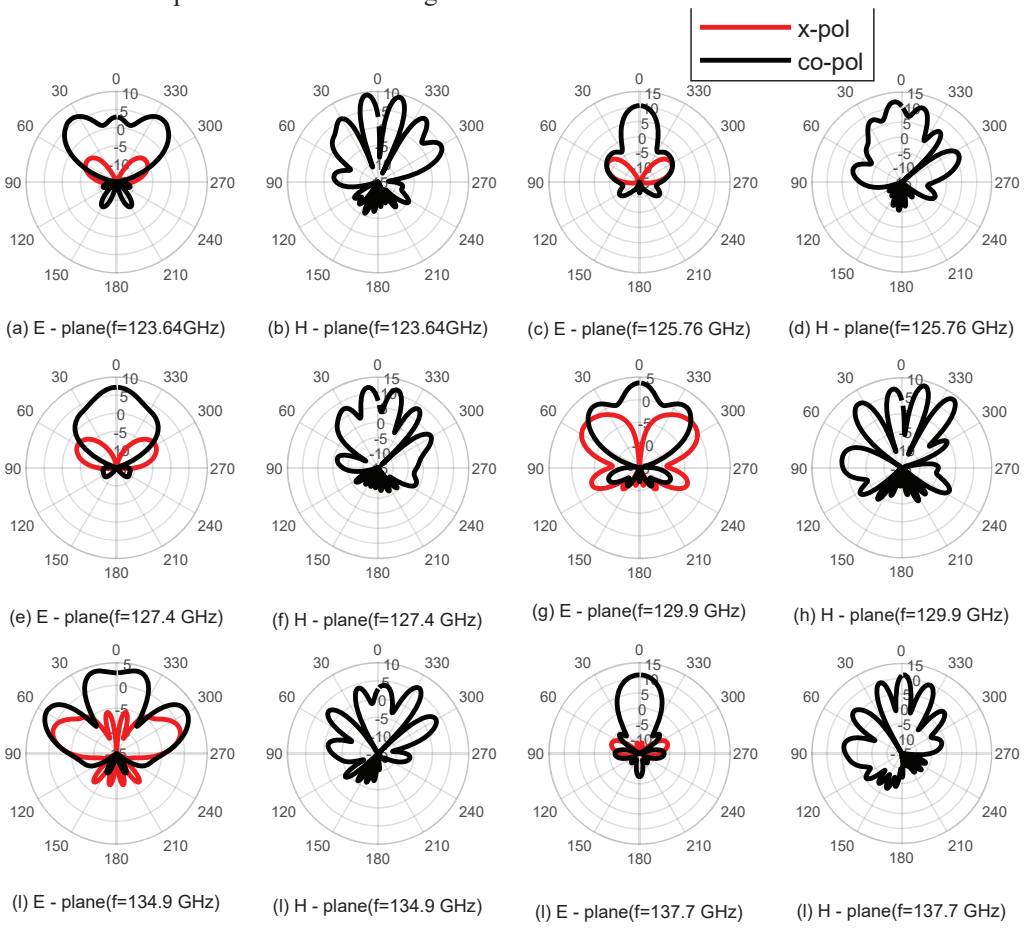

Fig. 4. Simulated radiation patterns in the E and H planes at 123.64 GHz, 125.76 GHz, 127.4 GHz, 129.9 GHz, 134.9 GHz and 137.7 GHz.

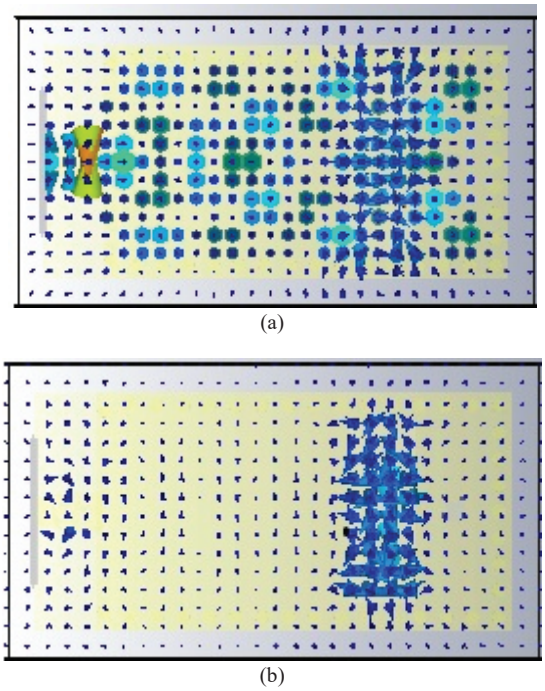

Fig 5. Simulated (a) E - field and (b) H - field of the proposed antenna at 125.76 GHz.

The increase in the level of the cross-polarization in the H-plane has been explained by [27] and [28] for a circular patch antenna and SIW-fed slot antenna respectively. In [27], there is evidence of experimental existence of orthogonally polarized E-fields (cross-polarization). This field is typically lower than the co-polarized fields while significantly increases in the H-plane. This phenomenon has been attributed to first higher order modes. Theoretical analysis has shown absolute absence of cross-polarized fields for an infinite ground plane. Therefore, low level of the cross-polarized field is as a result of the finite ground plane. Yi *et al* [28] have endeared to explain the phenomenon of increased co-polarized fields by observing the E and H-fields for an open slot antenna. Using a similar intuition, we analyze the electric and magnetic fields on the SIW section of the antenna. Fig. 5 shows these E and H-field distributions. The electric field is always vertical in the SIW section of the antenna. For a wave propagating down the waveguide, the direction of this field changes from vertical to horizontal at the slot. From Fig. 5, it can be observed that near the slot, the E-field is not purely horizontal while the H-field is not parallel to the open slot. These effects lead to cross polarized fields.

The enhancement in the bandwidth is attributed to the merging of higher order mode resonances. This is attributed to the improved impedance matching between the feeding line and the general antenna structure. To understand the contribution of these impedance matching techniques in broadening of the bandwidth, we describe the evolution of the antenna design stages. We define four different radiating structures. Antenna I is the initial design of the SIW-DRA formed as a result of optimizing the antenna parameters. The intermediate structure of the antenna with a DGS loaded on the ground plane is designated antenna II. Antenna III is formed by offsetting the vias from antenna I. Finally, by incorporating both techniques, the resulting radiation structure is designated antenna IV. These different antenna structures were simulated and their S_{11} performance compared. Fig. 6 shows the simulated reflection coefficients of the different radiating structures. It is observed that before the application of the impedance matching techniques, the antenna I operates in three different frequency bands (Band I - 122.29-123.84 GHz, band II - 124.53-134.65 GHz and band III - 137.1-140 GHz). It is noted that the effect of the offset via is to merge bands I and II, while the DGS is used to merge bands II and III.

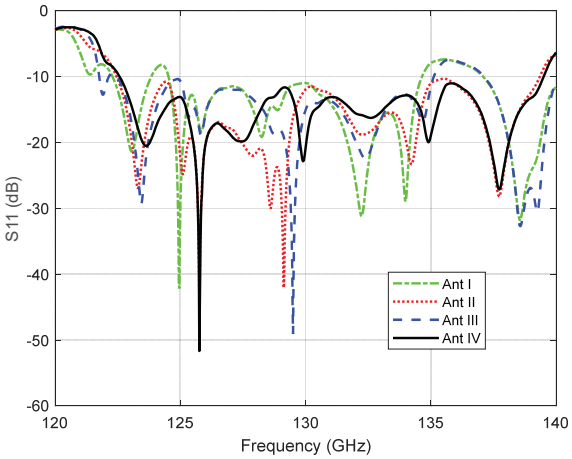

Fig 6. Simulated reflection coefficients for the different radiating structures.

As pointed out, the DGS disturbs the shield current distribution in the ground plane, altering the propagation of electromagnetic waves through the substrate layer. The slot has an effect of changing transmission line characteristics - capacitance and inductance of the antenna. This causes change in the antenna input impedance for improved matching. On the other hand, the offset via causes narrowing of the broad wall of the SIW at its input. This action is similar to the inductive iris type of discontinuity of metal waveguides. These discontinuities have been used for impedance matching. The offset vias behaves like a reactive energy storage elements. The vias excites higher order propagating modes in the waveguide. However, these modes are evanescent and are localized within the vicinity of the vias. This effect introduces a phase shift in the wave propagating in the SIW and cause impedance transformation to achieve improved impedance matching [29]. These have the effect of improving the impedance matching within this frequency band, therefore broadening the bandwidth to achieve a wideband antenna.

The contribution of the DGS and via offset to the antenna improvement can be observed by use of a smith chart. Fig. 7 shows the simulated plot of the loci of the reflection coefficients of different the antenna structures at different frequencies. Fig. 7(a) compares the loci of antenna I and antenna II between frequencies 134.6 GHz (points A and A') to points and 137.2 GHz (points B and B'). This is the range of frequencies separating bands II and III of antenna I, as

evident in Fig. 6. Etching out of the DGS on the ground place transforms the impedance in this frequency range, thus merging of bands II and III. From the plot, it is seen that the locus of antenna II (B-B') shrinks as compared to that of antenna I (A-A'), with a shift towards point (1+j0) on the chart, in the direction of the arrow. This shrinkage is associated with a reduction in the magnitude of reflection coefficients, indicating improved impedance matching. Similarly, Fig. 7(b) compares antenna I and antenna III between the high frequency of band I (123.8 GHz – points A-A') and the lower frequency of band II (124.6 – points B-B'). From Fig. 7(b), the locus of B-B' shows a reduction in magnitude of the reflection coefficient for antenna III compared to antenna I. However, there is a counter clockwise rotation, indicating a phase shift in the reflection coefficient. This can be attributed to the reactance of the offset via.

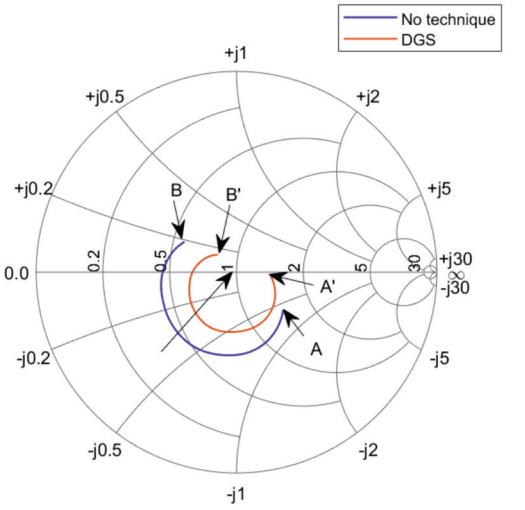

(a)

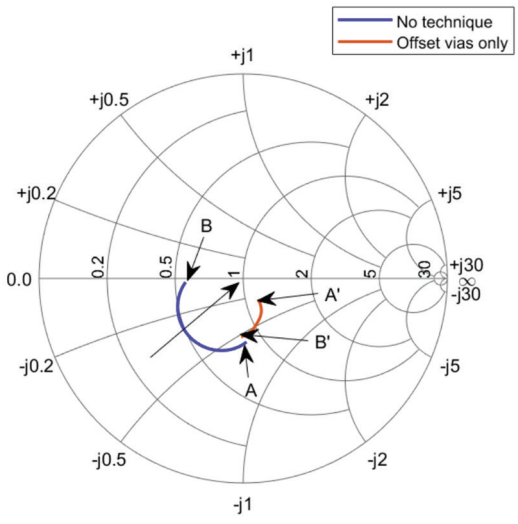

(b)

Fig 7. Simulated reflection coefficients of (a) antennas I and II at 134.6 GHz – 137.2 GHz and (b) antenna I and III at 123.8 GHz -124.6 GHz

The effects of the improved impedance matching on the radiation characteristics is further analyzed in terms of the main lobe magnitude and the side lobe levels (SLL) at the center frequency, for both the co-polarized and cross polarized fields. The main lobe magnitudes are observed to be 9.94 dBi, 10.1 dBi, 10 dBi and 10.3 dBi for the co-polarized E-plane fields and 0.437 dBi, -2.85 dBi, -3.36 dBi and -2.69 dBi for the cross polarized fields for the four radiating structures respectively. It is observed that both techniques enhances the co-polarized fields while suppressing the magnitudes of the cross polarized fields. The SLLs are given as -12.1 dB, -11.7 dB, -12.7 dB and -12.1 dB for the co-polarized fields and -24 dB, -24.2 dB, -24.5 dB and -25.6 dB for cross polarized fields for the different antenna structures. For the co-polarized fields, antenna II indicates a poor SLL performance as opposed to antenna III indicating the unsuitability of the DGS on SLL performance for the co-polarized fields. However, the application of both the DGS and via offset improves the SLL. For the cross polarized fields, antenna II and antenna III show a reduction in the SLLs. In conclusion, we note that the applied impedance matching techniques offer improved antenna performance, and as such are appropriate.

Fig. 8 shows the simulated plot of the variation of the voltage standing wave ratio (VSWR) against frequency. The VSWR is less than 2.0 within the band of operation, reaching a minimum of 1.006 at the resonant frequency of 125.76 GHz. The simulated gain of the antenna across the entire frequency of operation is also depicted in Fig 9. The antenna achieves a peak gain of 12.3 dBi at the frequency of 126 GHz.

Besides the gain, the directivity of the antenna is presented. Fig. 10 shows the 3D plot of the directivity of the antenna at 126 GHz. The antenna achieves a maximum directivity of 13.14 dBi at the frequency corresponding to maximum gain. The corresponding peak radiation efficiency is 84% at the same frequency. The inherently high efficiency is attributed to minimal conductor losses in DRA radiators.

To validate the proposed design, the antenna was modelled and simulated in Ansys HFSS software. These two softwares use different computational techniques whereby CST is a time-domain solver, whereas HFSS is a frequency-domain solver. Fig. 11 is a plot of the reflection coefficient generated from CST and HFSS. These are plotted on the same axes for performance comparison. The curves show agreement in terms of impedance bandwidth performance (122.58 GHz - 139.51 GHz for CST and 122.71 GHz - 139.69 GHz for HFSS) with the HFSS plot slightly shifted to the right. There is a shift in the center resonance frequency from 127.76 GHz to 130 GHz and a corresponding decrease in the minimum reflection coefficient at resonance from -50.63 dB to -32.84 dB for CST and HFSS results respectively. We further note that using HFSS, higher order resonances occur at frequencies close to those of the CST, with a slight upward shift. This difference is attributed to the different computational techniques employed.

Table III compares the results of the proposed design to the earlier works presented in [5], [11], [12], [14], [15], [30]-[32]. Antennas with similar feeding and radiation structures are compared so as to make inferences on the proposed design. It is observed that the proposed antenna offers the same impedance bandwidth to the antenna presented in [12] which

operates in the same frequency range. Despite antennas [15] and [30] offering an improved bandwidth and efficiency performance, its frequency of operation is lower than the proposed design. The performance of this design, in terms of antenna gain is superior to all the other earlier works.

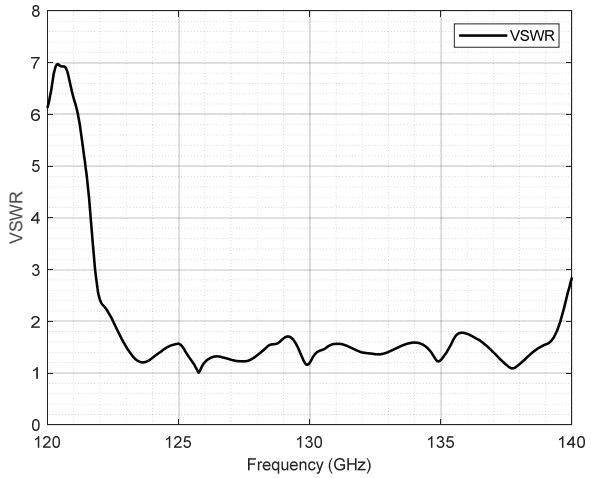

Fig 8. The simulated VSWR of the antenna

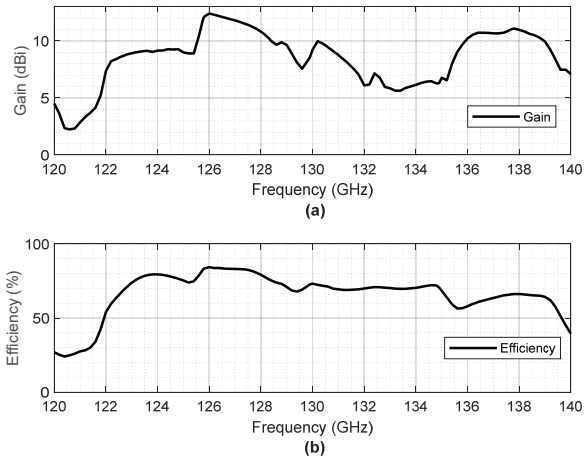

Fig 9. Graphs showing (a) Simulated gain and (b) Simulated efficiency against frequency

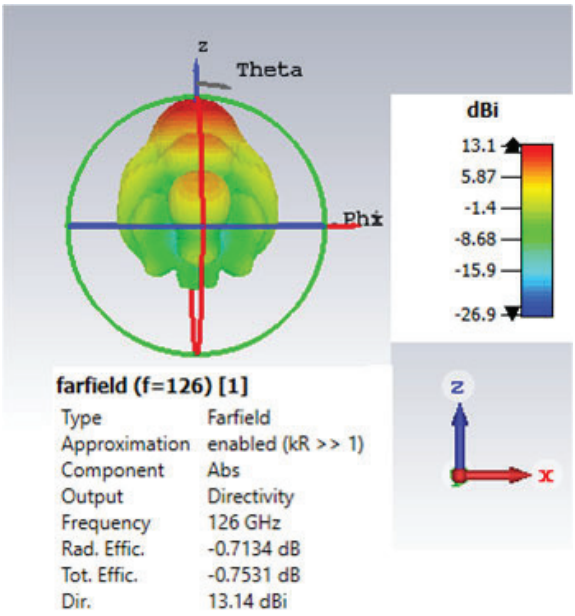

Fig 10. A 3D plot of the simulated directivity of the antenna at 126 GHz.

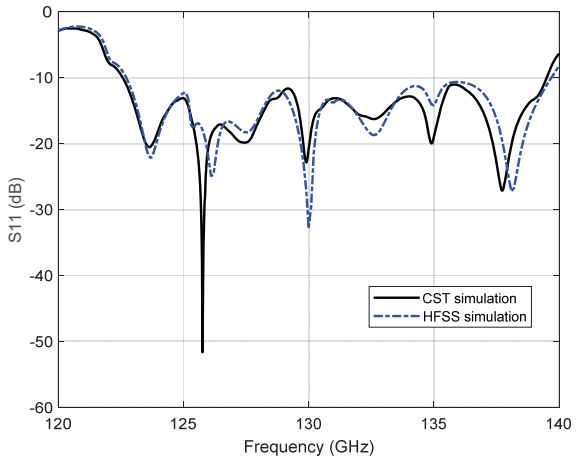

Fig 11. Performance comparison of the simulated reflection coefficients of the proposed design in CST and HFSS

TABLE III

PERFORMANCE COMPARISON OF THE PROPOSED ANTENNA WITH OTHER WORKS

Reference	Type	Feeding	Technique	f_0(GHz)	Bandwidth	Gain (dBi)	Efficiency
[30], 2010	CDRA	HMSIW	Cross slot feeding	60GHz	24.2%	5.5dB	92%
[31], 2014	RDRA	SIW	Modification of DRA	35	12%	5dBi	94%
[12] – Ant 3, 2014	On-chip RDRA	HMSIW	HOM	135	13%	3.7dBi	62%
[11], 2016	CDRA	SIW	Cross slot feeding	6.56	8.8%	3.7dB	-
[14], 2017	RDRA	SIW	Differential TE20 feeding	27.5-28.4	3.2%	4.2dBi	86%
[32], 2018	CDRA	SIW	HOM	25.8	2.15%	10.8dBi	87%
[15], 2021 – Band I	RDRA	SIW	HOM	24.5-27.5	24%	9.9dB	96%
Band II				33-37	12%	9.9dB	96%
[5], 2021	RDRA	SIW	Fractal geometry +HOM	5.74	19.5%	5.96dBi	-
This work	RDRA	SIW	HOM	125.67	13.4%	12.3dBi	84%

CDRA – Cylindrical DRA, HMSIW – Half Mode SIW, HOM – Higher Order Mode, RDRA – Rectangular DRA

IV. CONCLUSION

The design of a wideband SIW-DRA is proposed for application in the D – band frequency regime. The antenna operates from 122.58 GHz to 139.51 GHz with a -10 dB impedance bandwidth of 13.4% at a center frequency of 125.76 GHz. The wideband operation is as a result of merging of the higher order $TE_{10\delta1}$, $TE_{7\delta5}$, $TE_{\delta31}$, $TE_{\delta25}$, $TE_{\delta31}$ and $TE_{\delta35}$ resonant modes of the DR. This is achieved as a result of improved impedance matching of the antenna. Moreover, the antenna exhibits desirable attributes of high gain and efficiency, suitable for application in this frequency band.

REFERENCES

[1] Y. Shiroishi, K. Uchiyama and N. Suzuki, "Society 5.0: For Human Security and Well-Being," in *Computer*, vol. 51, no. 7, pp. 91-95, July 2018, doi: 10.1109/MC.2018.3011041.

[2] M. Maier, "6G as if People Mattered: From Industry 4.0 toward Society 5.0 : (Invited Paper)," *2021 International Conference on Computer Communications and Networks (ICCCN)*, pp. 1-10, 2021, doi: 10.1109/ICCCN52240.2021.9522181.

[3] Y. He, Y. Chen, L. Zhang, S. Wong and Z. N. Chen, "An overview of terahertz antennas," in *China Communications*, vol. 17, no. 7, pp. 124-165, July 2020, doi: 10.23919/J.CC.2020.07.011.

[4] I. Ali, M. H. Jamaluddin, A. Gaya and H. A Rahim, "A Dielectric Resonator Antenna with Enhanced Gain and Bandwidth for 5G Applications," *Sensors* 2020, *20*, 675. https://doi.org/10.3390/s20030675

[5] W. Luo, Y. Feng, Y. Ren and B. Yin, "A novel wideband fractal rectangular dielectric resonator antenna with improved radiation performance," *AEU - International Journal of Electronics and Communications*, vol. 142, 2021, https://doi.org/10.1016/j.aeue.2021.153984.

[6] R. K. Mongia and P. Bhartia, "Dielectric resonator antennas—a review and general design relations for resonant frequency and bandwidth." *Int. J. Microw. Mill.-Wave Comput.-Aided Eng.*, Vol 4. no. 3, pp.230-247. https://doi.org/10.1002/mmce.4570040304

[7] X. S. Fang and K. W. Leung, "Designs of Single-, Dual-, Wide-Band Rectangular Dielectric Resonator Antennas," in *IEEE Transactions on Antennas and Propagation*, vol. 59, no. 6, pp. 2409-2414, June 2011, doi: 10.1109/TAP.2011.2143658.

[8] T. Chang and J. Kiang, "Bandwidth Broadening of Dielectric Resonator Antenna by Merging Adjacent Bands," in *IEEE Transactions on Antennas and Propagation*, vol. 57, no. 10, pp. 3316-3320, Oct. 2009, doi: 10.1109/TAP.2009.2029372.

[9] R. Kumar Mongia and A. Ittipiboon, "Theoretical and experimental investigations on rectangular dielectric resonator antennas," in *IEEE Transactions on Antennas and Propagation*, vol. 45, no. 9, pp. 1348-1356, Sept. 1997, doi: 10.1109/8.623123.

[10] Y. -M. Pan, K. W. Leung and K. -M. Luk, "Design of the Millimeter-wave Rectangular Dielectric Resonator Antenna Using a Higher-Order Mode," in *IEEE Transactions on Antennas and Propagation*, vol. 59, no. 8, pp. 2780-2788, Aug. 2011, doi: 10.1109/TAP.2011.2158962.

[11] B. K. Thilagam, M. M Kartha and M. Jayakumar, "Performance analysis of cylindrical dielectric resonator antenna with various slot configurations on Substrate Integrated Waveguide," *IJCTA*, vol. 9, pp. 7581-7588, 2016.

[12] D. Hou *et al*., "D-band on-chip higher-order-mode dielectric-resonator antennas fed by half-mode cavity in CMOS technology," in *IEEE Antennas and Propagation Magazine*, vol. 56, no. 3, pp. 80-89, June 2014, doi: 10.1109/MAP.2014.6867684.

[13] M. Yang, Y. Pan, Y. Sun and K. Leung, "Wideband Circularly Polarized Substrate-Integrated Embedded Dielectric Resonator Antenna for Millimeter-Wave Applications," in *IEEE Transactions on Antennas and Propagation*, vol. 68, no. 2, pp. 1145-1150, Feb. 2020, doi: 10.1109/TAP.2019.2938629.

[14] A. Sharma, A. Sarkar, A. Biswas and M. J. Akhtar, "Millimeter-Wave Quad-Port Multiple-Input Multiple-Output Dielectric Resonator Antenna Excited Differentially by TE20 Mode Substrate Integrated Waveguide," *2019 URSI Asia-Pacific Radio Science Conference (AP-RASC)*, pp. 1-4, 2019,doi: 10.23919/URSIAP-RASC.2019.8738413.

[15] P. R. Girjashankar and T. Upadhyaya, "Substrate integrated waveguide fed dual band quad-elements rectangular dielectric resonator MIMO antenna for millimeter wave 5G wireless communication systems," *AEU - International Journal of Electronics and Communications*, vol. 137, 2021.

[16] G. Luo, X. Zhang, L. Dong, W. Li and L. Sun, "A Gain Enhanced Cavity Backed Slot Antenna using High Order Cavity Resonance," *Journal of Electromagnetic Waves and Applications - J ELECTROMAGNET WAVE APPLICAT*, vol 25, pp. 1273-1279, 2011, doi: 0.1163/156939311795762051.

[17] J. Wang, Z. -C. Hao and Kui-Kui Fan, "A 110–150 GHz SIW-rectangular waveguide transition for terahertz applications," *2016 IEEE MTT-S International Microwave Workshop Series on Advanced Materials and Processes for RF and THz Applications (IMWS-AMP)*, pp. 1-3, 2016, doi: 10.1109/IMWS-AMP.2016.7588309.

[18] Pozar, D. M., Microwave Engineering, 3rd Edition, Wiley, New York, USA, 2005

[19] J. E. Rayas-Sanchez and V. Gutierrez-Ayala, "A general EM-based design procedure for single-layer substrate integrated waveguide interconnects with microstrip transitions," *2008 IEEE MTT-S*

International Microwave Symposium Digest, pp. 983-986, 2008, doi: 10.1109/MWSYM.2008.4632999

[20] K. Wu, D. Deslandes and Y. Cassivi, "The substrate integrated circuits - a new concept for high-frequency electronics and optoelectronics," *6th International Conference on Telecommunications in Modern Satellite, Cable and Broadcasting Service, 2003. TELSIKS 2003.*, pp. P-III, 2003, doi: 10.1109/TELSKS.2003.1246173.

[21] A. Saxena, S. Joshi, A. Gupta, S. Saxena and D. Kumar, "Gain and bandwidth enhancement of CPW-fed patch antenna for wideband applications," *2016 IEEE International Conference on Recent Trends in Electronics, Information & Communication Technology (RTEICT)*, pp. 1622-1625, 2016, doi: 10.1109/RTEICT.2016.7808107.

[22] A. Petosa and S. Thirakoune, "Rectangular Dielectric Resonator Antennas With Enhanced Gain," in *IEEE Transactions on Antennas and Propagation*, vol. 59, no. 4, pp. 1385-1389, April 2011, doi: 10.1109/TAP.2011.2109690.

[23] Y. M. Pan, K. W. Leung and K. Lu, "Study of Resonant Modes in Rectangular Dielectric Resonator Antenna Based on Radar Cross Section," in *IEEE Transactions on Antennas and Propagation*, vol. 67, no. 6, pp. 4200-4205, June 2019, doi: 10.1109/TAP.2019.2911198.

[24] W. M. Abdel Wahab, D. Busuioc and S. Safavi-Naeini, "Low Cost Planar Waveguide Technology-Based Dielectric Resonator Antenna (DRA) for Millimeter-Wave Applications: Analysis, Design, and Fabrication," in *IEEE Transactions on Antennas and Propagation*, vol. 58, no. 8, pp. 2499-2507, Aug. 2010, doi: 10.1109/TAP.2010.2050443.

[25] P. Bhartia, Inder Bahl, R. Garg, A. Ittipiboon - Microstrip Antenna Design Handbook (Artech House Antennas and Propagation Library)-Artech House Publishers (2001)

[26] A. V. P. Kumar and A. K. Ojha, "Cross-Polarization Reduction of a Cylindrical Dielectric Resonator Antenna with Parasitic Strip Loading," *2018 International Conference on Signal Processing and Communications (SPCOM)*, 2018, pp. 139-142, doi: 10.1109/SPCOM.2018.8724476.

[27] C. Kumar and D. Guha, "Nature of Cross-Polarized Radiations from Probe-Fed Circular Microstrip Antennas and Their Suppression Using Different Geometries of Defected Ground Structure (DGS)," in *IEEE Transactions on Antennas and Propagation*, vol. 60, no. 1, pp. 92-101, Jan. 2012, doi: 10.1109/TAP.2011.2167921.

[28] X. Yi and H. Wong, "A Wideband Substrate Integrated Waveguide-Fed Open Slot Antenna," in *IEEE Transactions on Antennas and Propagation*, vol. 68, no. 3, pp. 1945-1952, March 2020, doi: 10.1109/TAP.2019.2948680.

[29] Robert E Collin_ IEEE Antennas and Propagation Society - Field theory of guided waves, 2nd Edition, IEEE Press, 1991

[30] Q. Lai, C. Fumeaux, W. Hong and R. Vahldieck, "60 GHz Aperture-Coupled Dielectric Resonator Antennas Fed by a Half-Mode Substrate Integrated Waveguide," in *IEEE Transactions on Antennas and Propagation*, vol. 58, no. 6, pp. 1856-1864, June 2010, doi: 10.1109/TAP.2010.2046852.

[31] K. Gong and X. H. Hu, "Low-Profile Substrate Integrated Dielectric Resonator Antenna Implemented With PCB Process," in *IEEE Antennas and Wireless Propagation Letters*, vol. 13, pp. 1023-1026, 2014, doi: 10.1109/LAWP.2014.2325033.

[32] M. Mrnka, M. Cupal, Z. Raida, A Pietriková and D. Kocur, "Millimeter-wave Dielectric Resonator Antenna Array Based on Directive LTCC Elements," *IET Microwaves, Antennas & Propagation*, pp. 662-667, January, 2018, doi: 10.1049/iet-map.2017.0492

Emmanuel K. Chemweno received his Bachelor of Science degree in Electrical and Electronics Engineering from Jomo Kenyatta University of Agriculture and Technology, Nairobi, Kenya in 2002 and a Master of Science degree in Electrical and Electronics Engineering from Jomo Kenyatta University of Agriculture and Technology, Nairobi, Kenya in 2019. He is currently studying for a PhD in Electronic Engineering at the University of KwaZulu-Natal, Durban, South Africa. His research interests are in the fields of Antennas and Microwave Engineering.

Pradeep Kumar received his Bachelor's degree in Electronics and Communication Engineering, Master of Engineering in Electronic and Communication Engineering and PhD in Electronics and Communications Engineering in 2003, 2005 and 2009, respectively. He completed his postdoctoral studies at the Autonoma University of Madrid, Spain. He has over 15 years of experience in academics and research. He has held various positions such as Lecturer, Senior Lecturer, Assistant Professor and Associate Professor. He is currently working with the University of Kwazulu-Natal, South Africa. His research interests are in the fields of Antenna Design, Wireless Communications, Signal and Image Processing.

Thomas J. O. Afullo received his Bachelor's degree in Electrical and Electronic Engineering (Hons) from The University of Nairobi, Kenya in 1979, MSEE from The University of West Virginia, USA in 1983 and PhD in Telecommunication Engineering from Vrije Universiteit (VUB), Belgium in 1989. He worked with Kenya Posts and Telecommunications Corporation (1981-1986), rising to the position of Senior Executive Engineer. He was with Moi University, Kenya (1986 – 1994), University of Botswana (1996 – 2002) and UDW/UKZN, South Africa (2003 – date). He is currently a Professor and Director for Centre for Radio Access and Rural Technology (CRART) in the Discipline of Electrical, Electronic and Computer Engineering at the University of KwaZulu-Natal, Durban, South Africa. He is a member of the Eta Kappa Nu (MHKN), Senior Member, IEEE and a fellow of the South African Institute of Electrical Engineers (FSAIEE). His research interests are in the area of Microwave and Millimeter-wave propagation, Power Line Communications (PLC) and Free Space Optics (FSO).

CONTENTS PAGE